A Global Catalogue of Lunar Topographic Prominence ≥ 1 km

Jim Singh[1], Daniel Quinn[2*] and Oscar Argudo[3]

[1]*Independent Researcher*
[2]*Independent Researcher*
[3]*Associate Professor, Universitat Politècnica de Catalunya*
[*]*Corresponding author: Daniel Quinn* – dan@gunung.org

Abstract

We present the Lunar Ribus Database, a global catalogue of lunar summits with topographic prominence ≥1 km derived from the highest-resolution global and regional digital elevation models currently available. Each summit in the catalogue is reported with summit and key col elevations relative to the global minimum, prominence, key col elevation, and geographic coordinates of both summit and key col. Prominence was computed using the divide-tree algorithm of Andrew Kirmse (*mountains*).

Summits with prominence ≥1 km, called Ribus, provide a formal measure of morphometric independence. By linking each summit to its key col, the Lunar Ribus Database establishes a globally consistent hierarchy of kilometre-scale positive-relief landforms on the Moon. This framework enables terrain segmentation, analysis of impact- and volcanism-related edifices, and comparative prominence-based morphometry across planetary bodies.

1. Introduction

Topographic prominence provides a parameter-free measure of morphometric independence. Unlike height above local terrain or break-in-slope detection methods, prominence is defined solely by the geometry of the digital elevation model and the connectivity of the surface through its lowest linking saddles.

Because it captures the hierarchical structure of relief directly from topography, this metric has proven valuable for quantifying and characterising landforms across a range of settings. For example, the United States Geological Survey has applied prominence-based methods to convert terrestrial summit features from point representations in the Geographic Names Information System into spatially bounded landforms (Sinha & Arundel, 2020). Its use in planetary geomorphology includes basin-ring reconstruction on the Moon (Bailey et al., 2020), vent identification on the Moon (Cañón-Tapia & Jacobo-Bojorquez, 2022), volcanic edifice characterisation on Mars (Richardson et al., 2021), and segmentation of highland terrain on Venus (Kiefer et al., 1991).

However, such applications have been limited to regional investigations or to specific classes of landforms. To our knowledge, no globally consistent inventory of prominent summits has been compiled for any planetary body other than Earth.

Here we present a global catalogue of lunar positive-relief features with topographic prominence ≥1 km derived from modern digital elevation models. Landforms exceeding this threshold correspond to the “sub-Ultra” prominence class discussed by Walsh et al. (2022) in their analysis of South Pole-Aitken basin massifs.

In this work, lunar summits with prominence ≥1 km are referred to as Ribu (singular) and Ribus (plural), from the Indonesian and Malay word *ribu* meaning “thousand”. The informal designation “sub-Ultra” for summits of this prominence range has not been widely adopted in the literature. The term Ribu is therefore used here as a concise label for kilometre-prominence summits and is applied consistently across a growing set of planetary Ribus catalogues currently under development (World Ribus Project, 2026).

2. Topographic Data Sources

Elevations for the Lunar Ribus Database (Academic Release; hereafter “Lunar Ribus Database”) were derived from a hierarchy of lunar digital elevation models, selecting the highest-resolution dataset available at each location.

Where available, NAC stereo DEMs (2-5 m/pixel) were used; these occur as localised regional products derived from imaging by the Lunar Reconnaissance Orbiter Narrow Angle Camera (Robinson et al., 2010).

For locations poleward of 60° latitude, elevations were taken from a polar DEM derived from the Lunar Orbiter Laser Altimeter (LOLA; Smith et al., 2010). LOLA altimetry has been compiled into global grids at multiple resolutions (Planetary Data System, 2026); the DEM used here has a resolution of ~60m/pixel. In these products, data gaps are interpolated using splines under tension (Smith and Wessel, 1990), which suppress unrealistic topographic artifacts in sparsely sampled regions while preserving the large-scale structure of the surface. Within ±60° latitude, elevations were obtained from the SLDEM2015 global DEM (Barker et al., 2016). This model integrates LOLA altimetry with parallax-derived topography from the SELENE Terrain Camera (TC), using TC stereo data to correct geolocation errors in LOLA and to replace interpolated regions with measured topography. The resulting DEM preserves the ~60m/pixel resolution of the LOLA grid, with the higher-resolution TC imagery downsampled to match the global topographic scale (Fernandes and Mosegaard, 2022).

Elevations are referenced to the lowest resolved natural surface point on the Moon rather than to an adopted mean planetary radius. This ties the vertical datum directly to an observed surface location rather than a geometric reference sphere and avoids dependence on externally adopted lunar radii. Summit elevations, key col elevations, and prominences are therefore expressed within a consistent geometric framework defined by the topographic datasets used in the analysis.

All feature coordinates are expressed in planetocentric latitude and longitude, consistent with the source DEMs. Longitudes have been normalised to the -180° to +180° convention, with negative values indicating west and positive values east.

3. Methods

Prominence was calculated using the C++ divide-tree algorithm developed by Andrew Kirmse (*mountains*), which implements a global saddle-based prominence computation derived from the framework used in WinProm (Earl, 2012). The method treats the digital elevation model as a continuous surface and derives summit-saddle relationships from the connectivity of the terrain.

The procedure consists of the following steps:

3.1. Summit detection

Summits are identified as local maxima surrounded by lower terrain, independent of the magnitude of the surrounding elevation difference. Each such maximum represents a candidate summit.

3.2. Saddle detection

Saddles are identified as locations surrounded by alternating higher and lower terrain, with at least two higher and two lower neighbouring regions. These points represent the lowest passes linking adjacent summit domains.

3.3. Divide-tree construction

For each saddle, the algorithm follows the direction of steepest ascent from the saddle into each adjacent higher region until a summit is reached. These saddle-to-summit connections form a graph linking summits through their intervening passes. If closed loops arise within this graph, the lowest saddle within the loop and its associated connections are removed, ensuring that the resulting structure forms a hierarchical divide tree.

3.4. Key col identification

From each summit, the divide tree is traversed toward higher summits. The lowest saddle encountered along such a path represents a candidate key col. When multiple paths to higher summits exist, several candidate saddles may be identified; the highest of these candidates defines the summit's true key col.

On Earth, the key col of the planet's highest summit is implicitly sea level, providing a natural external reference. In contrast, a closed surface without oceans, such as the Moon, has no such reference level, and the highest summit has no higher neighbour from which a key col can be derived. To maintain a finite and internally consistent prominence hierarchy, we adopt the convention that the Moon's highest summit and the second most prominent summit share the same key col. This convention follows directly from the divide-tree interpretation of prominence and preserves the mathematical structure of the hierarchy.

3.5. Prominence computation

Topographic prominence is calculated as the elevation difference between a summit and its key col.

3.6. Summit selection

Summits are retained in the final catalogue if their computed prominence exceeds the adopted threshold.

3.6.1. Prominence threshold

A minimum prominence threshold of $P \geq 1$ km was adopted for summit selection. This value was guided by a combination of geomorphological and practical considerations, as follows:

- Noise suppression: High-frequency lunar topographic roughness produces landforms with several hundred metres to ~1 km of relief across degraded crater rims, ejecta hummocks, and overlapping impact structures. Including these abundant small-scale landforms in a morphometric inventory can obscure morphometrically independent landforms (Walsh et al., 2023).

- Structural significance: Features with P ≥ 1 km correspond to mechanically coherent morphologic units such as massifs, well-developed central peaks, and basin-ring elements.

- Dataset tractability: The 1 km threshold yields 3670 qualifying summits - sufficient to capture global morphostructural patterns while remaining computationally and analytically manageable. Lower thresholds would significantly increase the catalogue size.

3.6.2. Initial screening threshold

During the initial analysis a provisional prominence threshold of P ≥ 900 m was used as a screening step. This allowed candidate features close to the kilometre-prominence threshold to be retained while elevations were cross-checked across multiple digital elevation models. Differences in DEM resolution, interpolation or local data coverage can shift computed prominences by several tens of metres. Including features slightly below the final cutoff ensured that summits potentially exceeding P ≥ 1 km in higher-resolution or alternative datasets were examined during validation. The final catalogue retains only those summits confirmed to exceed 1 km prominence after this verification process.

3.7. Naming of features

Lunar features officially named by the International Astronomical Union (IAU) are recorded in uppercase. Summits in the catalogue lacking an official name have been assigned provisional lowercase names, following a structured convention. In most cases, unnamed summits are associated with the nearest officially named lunar feature, typically an impact crater. Individual summits are distinguished using Greek-letter suffixes, ordered by prominence. The use of Greek letters follows lunar cartography tradition, where they have historically been used to label subsidiary features around named craters. Where a summit represents a clearly distinct morphologic unit, such as a central peak or massif within a crater, a Mons prefix may be used. In a small number of cases, identifiers already used informally in astronomical literature or mapping resources are adopted where these can be applied unambiguously.

Each feature is also assigned a unique catalogue identifier consisting of the prefix L (for *Luna*/ lunar) followed by four digits (e.g., L1234). These identifiers provide a stable reference

for catalogue records independent of provisional naming. The provisional names and identifiers are intended solely for use within the catalogue and do not constitute formal nomenclature.

3.8. Geospatial visualisation

To show the geospatial structure of the catalogue and the summit-key col relationships that define prominence, the catalogue was converted to GeoJSON format and visualised in Lunar Quickmap (NASA et al., 2026), as shown in Figures 1-3.

The top panel of Figure 1 shows a lunar mountain-range that serves as a real-world counterpart to the prominence relationships depicted in Sinha & Arundel (2020).

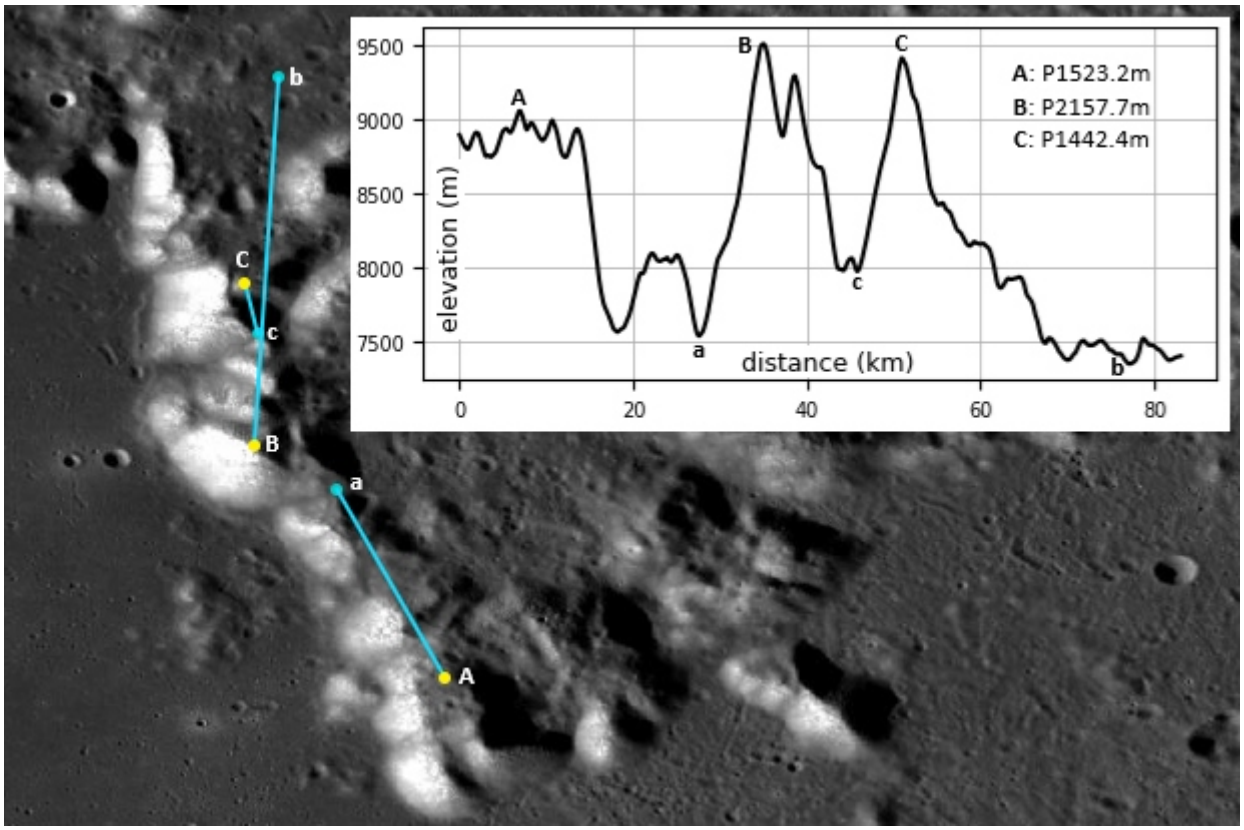

Figure 1. Lunar Ribus Database displayed as a GeoJSON layer in Lunar Quickmap. Yellow points denote summits, blue points denote key cols, and blue line segments connect each summit to its corresponding key col. Seen here is an enlarged view of the southern tip of MONTES ALPES. Labeled features are (A) PROMONTORIUM AGASSIZ, (B) PROMONTORIUM DEVILLE, and (C) Cassini P Alpha. The inset shows an elevation profile along a multi-segment transect connecting each summit and its associated key col, and displays the prominence of each summit.

In the complex-crater example of Figure 2, the prominence (A-a) of the central peak corresponds to its height above the crater floor, and prominence (B-b) corresponds to rim height above the surrounding terrain. Unlike break-in-slope methods (e.g., Bray et al., 2008) or DEM-histogram approaches (e.g., Kalynn et al., 2013) which require definitions of "floor," "rim," or "pre-impact terrain," prominence derives these relationships solely from the summit-col pair. This makes it both complementary to those techniques and uniquely base-independent, while also encoding the morphometric independence of each summit.

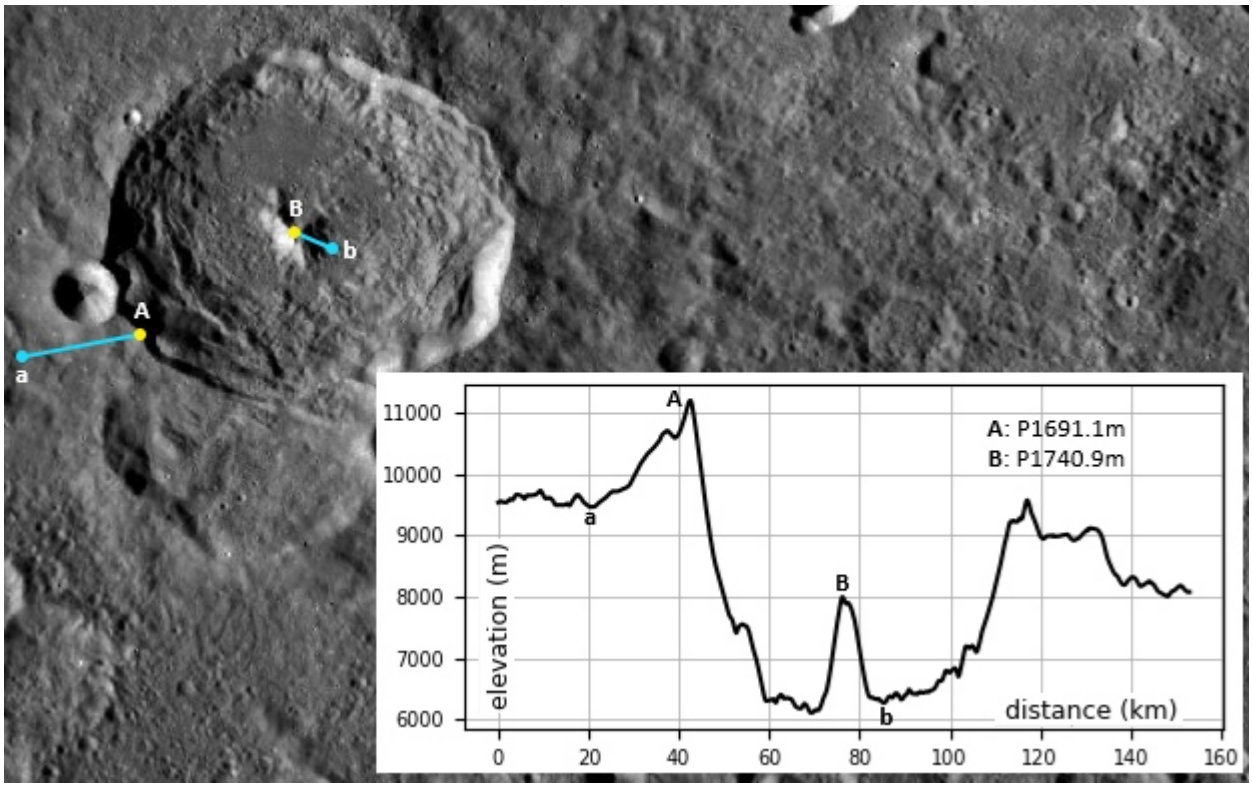

Figure 2. Plutarch crater. Labeled features are (A) Plutarch Beta, (B) Mons Plutarch. The inset elevation profile across the crater shows these as a rim Ribu and a central-peak, respectively.

Figure 3 depicts the distribution of Ribus in a nearside mare region, demonstrating that key cols may occur over a wide range of positions and separations relative to their summits.

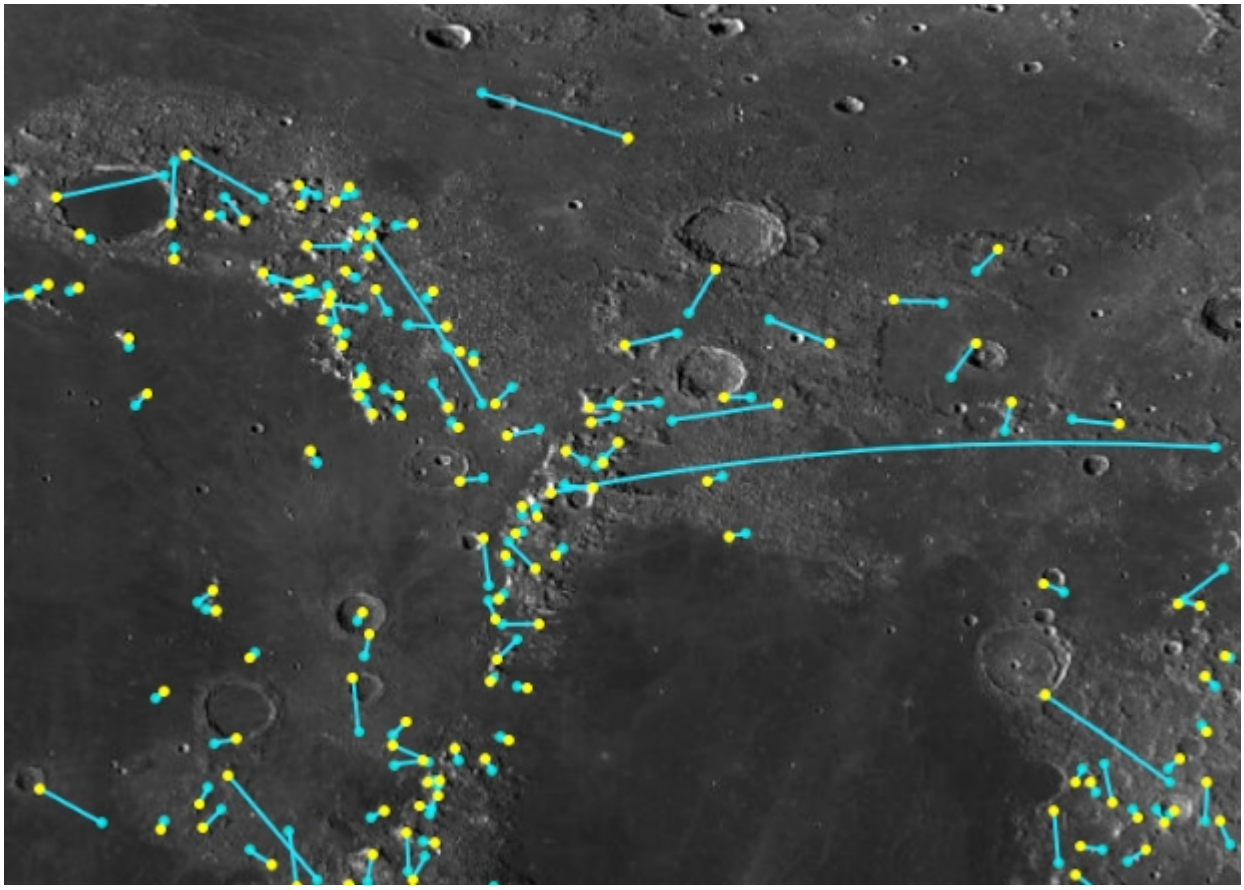

Figure 3. Regional view extending beyond the MONTES ALPES area of Figure 1, showing a broader distribution of summits and their key cols. The longest connector visible corresponds to the summit-key col pair of the most prominent summit within the Imbrium Basin rings system: Mons Calippus C / Mons Elbruz.

4. Lunar Ribus Database

4.1. Contents

Each record contains:

- Unique ID number
- Summit name
- Summit latitude (°) and longitude (°)
- Summit elevation (m)
- Key col latitude (°) and longitude (°)

- Key col elevation (m)
- Topographic prominence (m)

4.2. Availability

The Lunar Ribus Database is provided as a comma-separated values (CSV) file containing one record per summit. It is archived on Zenodo and is accessible via DOI: https://doi.org/10.5281/zenodo.19363869. Users of the catalogue are requested to cite the catalogue DOI.

4.3. Applications

The Lunar Ribus Database enables:

- Hierarchical morphostructural classification
- Quantification of central uplifts in impact craters
- Basin-ring and massif segmentation
- Identification of mechanically independent crustal blocks
- Prominence-frequency distribution analysis
- Base-independent edifice height measurement
- Integration with IAU lunar nomenclature datasets

5. Conclusion

The Lunar Ribus Database provides a reproducible, globally consistent morphometric framework for kilometre-scale positive relief on the Moon. It establishes a structural basis for quantitative analysis of lunar topography and offers a foundation for comparative prominence studies across planetary bodies.

References

Bailey, A. M., Wagner, R. V., & Robinson, M. S. (2020). Mountain by mountain: Defining lunar basins. *In Proceedings of the 51st Lunar and Planetary Science Conference* (Abstract 1753).

Barker, M. K., Mazarico, E., Neumann, G. A., Zuber, M. T., Haruyama, J., & Smith, D. E. (2016). A new lunar digital elevation model from the Lunar Orbiter Laser Altimeter and SELENE Terrain Camera. *Icarus*, *273*, 346-355. https://doi.org/10.1016/j.icarus.2015.07.039

Bray, V. J., Collins, G. S., Morgan, J. V., & Schenk, P. M. (2008). The effect of target properties on crater morphology: Comparison of central peak craters on the Moon and Ganymede. *Meteoritics & Planetary Science*, *43*(12), 1979-1992. https://doi.org/10.1111/j.1945-5100.2008.tb00656.x

Cañón-Tapia, E., & Jacobo-Bojorquez, R. A. (2022). Sub-volcanic structure beneath Marius Hills, Moon, inferred from vent distribution. *Journal of Geophysical Research: Planets*, *127*, e2021JE006960. https://doi.org/10.1029/2021JE006960

Earl, E. (2012). *WinProm: Software for computing topographic prominence*. https://github.com/edwardearl/winprom

Fernandes, I., & Mosegaard, K. (2022). High-resolution topography from planetary images and laser altimetry. *Planetary and Space Science*, *218*, 105514. https://doi.org/10.1016/j.pss.2022.105514

Kalynn, J., Johnson, C. L., Osinski, G. R., & Barnouin, O. (2013). Topographic characterization of lunar complex craters. *Geophysical Research Letters*, *40*(1), 38-42. https://doi.org/10.1029/2012GL053608

Kiefer, W. S., & Hager, B. H. (1991). A mantle plume model for the equatorial highlands of Venus. *Journal of Geophysical Research: Planets*, *96*(E4), 20947-20966. https://doi.org/10.1029/91JE02221

Kirmse, A. (n.d.). *mountains: Divide-tree algorithm for computing topographic prominence*. https://github.com/akirmse/mountains

NASA, Arizona State University, & Applied Coherent Technology Corp. (2026). *Lunar QuickMap*. https://quickmap.lroc.im-ldi.com/ (accessed March 2026).

Planetary Data System. (2026). *LOLA gridded data records (GDR), cylindrical projection*. Lunar Reconnaissance Orbiter. https://pds-geosciences.wustl.edu/lro/lro-l-lola-3-rdr-v1/lrolol_1xxx/data/lola_gdr/cylindrical/img/ (accessed March 2026).

Richardson, J. A., Bleacher, J. E., Connor, C. B., & Glaze, L. S. (2021). Small volcanic vents of the Tharsis volcanic province, Mars. *Journal of Geophysical Research: Planets*, *126*(2), e2020JE006620. https://doi.org/10.1029/2020JE006620

Robinson, M. S., Brylow, S. M., Tschimmel, M. E., Humm, D., Lawrence, S. J., Thomas, P. C., Denevi, B. W., Bowman-Cisneros, E., Zerr, J., Ravine, M. A., & Caplinger, M. A. (2010). Lunar Reconnaissance Orbiter Camera (LROC) instrument overview. *Space Science Reviews*, *150*(1), 81-124. https://doi.org/10.1007/s11214-010-9634-2

Sinha, G., & Arundel, S. T. (2020). Automated extraction of areal extents for GNIS summit features using the eminence core method. In *Proceedings of the Geomorphometry 2020 Conference* (pp. 38-41). https://doi.org/10.30437/GEOMORPHOMETRY2020_10

Smith, D. E., Zuber, M. T., Jackson, G. B., Cavanaugh, J. F., Neumann, G. A., Riris, H., Sun, X., Zellar, R. S., Coltharp, C., Connelly, J., & Katz, R. B. (2010). The Lunar Orbiter Laser Altimeter investigation on the Lunar Reconnaissance Orbiter mission. *Space Science Reviews*, *150*(1), 209-241. https://doi.org/10.1007/s11214-009-9512-y

Smith, W. H. F., & Wessel, P. (1990). Gridding with continuous curvature splines in tension. *Geophysics*, *55*(3), 293-305. https://doi.org/10.1190/1.1442837

Walsh, J. M., Bailey, A. M., Bernhardt, H., Boyd, A. K., Wagner, R. V., Henriksen, M. R., & Robinson, M. S. (2022, June). Identification and applications of South Pole-Aitken Basin massifs. In *Proceedings of the 2022 Annual Meeting of Planetary Geologic Mappers* (Vol. 2684, p. 7046).

Walsh, J. M., Bailey, A. M., Boyd, A. K., Bernhardt, H., Wagner, R. V., Henriksen, M. R., Robinson, M. S., & Edwards, C. S. (2023). Preliminary South Pole-Aitken Basin ring reconstruction using massifs. In *Proceedings of the 54th Lunar and Planetary Science Conference* (LPI Contribution No. 2806, p. 1684).

World Ribus Project. (2026). *Other worlds Ribus catalogues*. https://spaceribus.pythonanywhere.com; https://worldribus.org/other-worlds-blog/ (accessed March 2026).